

ASME Journal of Dynamic Systems, Measurement, and Control Online journal at:

https://asmedigitalcollection.asme.org/dynamicsystems



Chrysostomos Karakasis

Department of Mechanical Engineering, University of Delaware, Newark, DE 19716 e-mail: chryskar@udel.edu

Ioannis Poulakakis

Department of Mechanical Engineering, University of Delaware, Newark, DE 19716 e-mail: poulakas@udel.edu

Panagiotis Artemiadis¹

Department of Mechanical Engineering, University of Delaware, Newark, DE 19716 e-mail: partem@udel.edu

An Energy-Based Framework for Robust Dynamic Bipedal Walking Over Compliant Terrain

Bipedal locomotion over compliant terrain is an important and largely underexplored problem in the robotics community. Although robot walking has been achieved on some nonrigid surfaces with existing control methodologies, there is a need for a systematic framework applicable to different bipeds that enables stable locomotion over various compliant terrains. In this work, a novel energy-based framework is proposed that allows the dynamic locomotion of bipeds across a wide range of compliant surfaces. The proposed framework utilizes an extended version of the 3D dual spring-loaded inverted pendulum (Dual-SLIP) model that supports compliant terrains, while a bio-inspired controller is employed to regulate expected perturbations of extremely low ground-stiffness levels. An energy-based methodology is introduced for tuning the bio-inspired controller to enable dynamic walking with robustness to a wide range of low ground-stiffness one-step perturbations. The proposed system and controller are shown to mimic the vertical ground reaction force (GRF) responses observed in human walking over compliant terrains. Moreover, they succeed in handling repeated unilateral stiffness perturbations under specific conditions. This work can advance the field of biped locomotion by providing a biomimetic method for generating stable human-like walking trajectories for bipedal robots over various compliant surfaces. Furthermore, the concepts of the proposed framework could be incorporated into the design of controllers for lower-limb prostheses with adjustable stiffness to improve their robustness over compliant surfaces.

[DOI: 10.1115/1.4064094]

Keywords: biped, locomotion, 3D Dual-SLIP, compliant, stiffness, energy

1 Introduction

Despite significant advances in the design of bipedal robots, most existing control methodologies focus primarily on locomotion over rigid terrain [1]. In real-world applications though, bipedal robots often encounter unforeseen non-rigid terrains with highly variable ground properties [2,3]. Therefore, in contrast to humans who are considered the "gold standard" of robotic-legged locomotion, consistent performance and safety cannot be guaranteed [4]. As a result, the need emerges for a terrain-specific framework that enables stable locomotion with robustness to various compliant terrains.

In previous works, bipedal robots have been exposed to compliant surfaces to validate the robustness of proposed control frameworks, in both simulation and real experiments [5–8]. Nonetheless, only distinct existing and simulated compliant terrains have been tested, hence limiting the claimed robustness. On the other hand, several control approaches have taken into account the terrain dynamics by modeling the foot-ground interaction through simple and more complex models [9–12]. Although some of these methods enabled locomotion of passive models and underactuated robots over a wide range of compliant surfaces, they are not scalable or generalizable to

estimating the terrain parameters (e.g., stiffness) and classifying the terrain type, which could potentially allow the employment of distinct control strategies for specific terrains [1,2,13]. As a result, there is a need for a general control framework applicable and scalable to different bipeds that models the ground properties and enables robust locomotion over various compliant terrains.

Previous research efforts employed simple mechanical "templates" to understand fundamental properties of locomotion

other bipeds, as they rely on specific robot or model structures and parameters. Furthermore, recently developed methods focus on

"templates" to understand fundamental properties of locomotion for highly complicated-legged robots and organisms, including single and double-legged robots, as well as people with or without amputation [14–19]. The 2D dual spring-loaded inverted pendulum (Dual-SLIP) model stands out against other models of human walking, due to its human-like center of mass (CoM) vertical oscillations and vertical ground reaction force (GRF) responses [20]. In addition, the model has also been very useful for robotics due to its ability to describe the double support periods inherent in human walking and to support online planning [21,22]. A threedimensional version of the model (3D Dual-SLIP) capable of producing human-like CoM lateral sway has also been proposed [21]. Although control approaches based on actuated variations of the 3D Dual-SLIP model have addressed walking on rigid, rough, and uneven surfaces [23,24], the behavior of the 3D Dual-SLIP model over compliant surfaces has not been studied.

The leg stiffness of legged robots and models has been shown to be critically associated with their robustness to perturbations and

¹Corresponing author.

Contributed by the Dynamic Systems Division of ASME for publication in the JOURNAL OF DYNAMIC SYSTEMS, MEASUREMENT, AND CONTROL. Manuscript received June 27, 2023; final manuscript received November 6, 2023; published online December 11, 2023. Assoc. Editor: Vaibhav Srivastava.

disturbances, as well as their energy consumption [10,11,25-34]. In Refs. [25-27], the leg stiffness of planar monopedal and bipedal spring-mass models was found to be associated with self-stability and robustness against perturbations in the system's state and terrain height variations. In Refs. [28–30], the 2D Dual-SLIP model was extended to have variable leg stiffness, resulting in the bipedal variable SLIP (V-SLIP) model. Moreover, control strategies adjusting the leg stiffness of the V-SLIP have been shown to stabilize the model, improve its robustness to external force disturbances, allow it to switch between different walking speeds, and improve energy efficiency. Recently, this model was further extended by adding actuated ankle joints and finite-sized feet, which allowed for increased step length during walking compared to the traditional 2D Dual-SLIP model [33]. Lastly, adjusting the hip torsional stiffness of a planar passive walker was shown to improve adaptability in different and varying compliant environments [10,11]. In addition to the above simulation-based works, the importance of leg stiffness has also been demonstrated in actual designs, where adjusting leg stiffness has been shown to improve the energy efficiency and robustness to perturbations of monopedal robots [31,32,34]. In summary, the adjustment of leg stiffness is shown to improve robustness and reduce energy expenditure in legged systems walking on both rigid and non-rigid terrains.

According to biomechanics research, humans and birds adjust the stiffness of their legs based on ground stiffness [35–38]. More specifically, it was found that when humans hop or run on surfaces of different stiffness, leg stiffness increases for decreasing ground stiffness values [35,36]. Moreover, it has been shown that runners increase leg stiffness when transitioning from hard to softer surfaces [37]. Similarly, guinea fowl exhibit increased leg stiffness when running down a visible step [38]. Therefore, previous research in biomechanics further motivates the exploitation of leg stiffness adjustments to achieve locomotion over compliant surfaces.

In this work, a novel energy-based framework is proposed that allows the dynamic locomotion of bipeds across various compliant surfaces. The proposed framework utilizes an extended variation of the 3D Dual-SLIP model and a bio-inspired controller that adjusts the leg stiffness of the model to achieve stable walking with robustness to extremely low ground-stiffness perturbations [39]. Specifically, the bio-inspired controller has led to stable locomotion after expected one-step unilateral ground-stiffness perturbations at stiffness levels as low as $30 \, kN/m$ [39], resembling the ground stiffness of a foam pad [40]. An energy-based methodology is introduced for tuning the bio-inspired controller to enable dynamic locomotion with robustness to a wide range of low-stiffness unilateral one-step perturbations. Additionally, the similarity between the GRF responses observed in humans and the proposed model is investigated, and the performance of the controller under repeated stiffness perturbations is explored. It must be noted that the proposed framework can generate reference trajectories for a wide variety of biped robots, without requiring these robots to have adjustable leg stiffness. These results can advance the field of bipedal locomotion, by providing stable reference trajectories to bipeds and humanoids traversing compliant terrains, as well as improving the robustness of prosthetic devices with tunable stiffness [41–43].

2 Materials and Methods

A variation of the three-dimensional biped walking 3D Dual-SLIP model was recently proposed to address locomotion over compliant surfaces [39]². There, a novel bio-inspired controller was proposed to handle expected one-step unilateral perturbations of

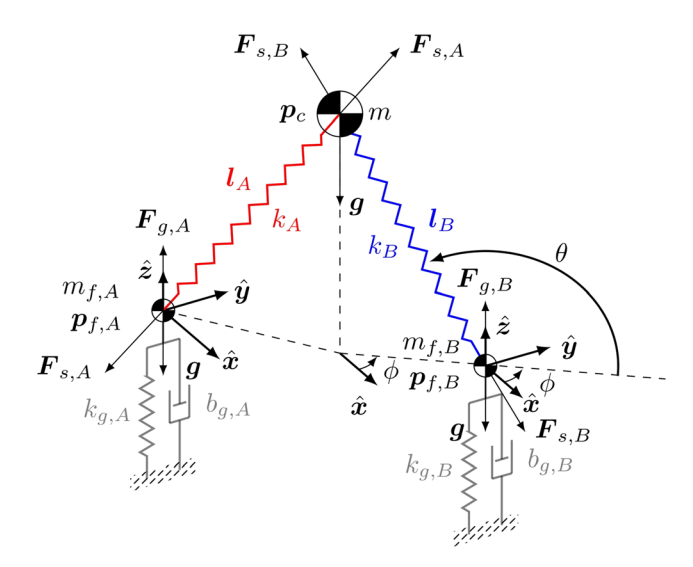


Fig. 1 The extended 3D Dual-SLIP model previously proposed to support locomotion over compliant surfaces [39]

extremely low ground stiffness. Both the extended model and the bio-inspired controller are briefly analyzed in this section, while the energy conservation of the system is explored in depth, together with its relation to tracking accurately periodic symmetric walking gaits.

2.1 The Extended 3D Dual-Spring Loaded Inverted Pendulum Model. A variation of the 3D Dual-SLIP model was recently proposed that supports locomotion over compliant surfaces, whilst maintaining its human-like properties, such as vertical CoM oscillations, vertical GRF responses, and lateral sway [39]. As shown in Fig. 1, the model consists of a point mass supported by two massless spring legs with foot masses attached to their endpoints. Specifically, m > 0 denotes the point mass, $\mathbf{p}_c = [x_c \quad y_c \quad z_c]^\top \in \mathbb{R}^3$ the CoM position, while for each leg $i \in \{A, B\}$, $\mathbf{p}_{f,i} = [x_{f,i} \quad y_{f,i} \quad z_{f,i}]^\top \in \mathbb{R}^3$ represents the foot position, k_i the leg stiffness, $m_{f,i}$ the foot mass, and $l_i = \mathbf{p}_c - \mathbf{p}_{f,i} \in \mathbb{R}^3$ the vector spanning from the foot to the point mass; both legs share the same rest length $l_0 > 0$ of this vector. Similarly in Ref. [39], $\theta \in \mathbb{R}$ and $\phi \in \mathbb{R}$ denote the forward and lateral touchdown angles, respectively³.

The 3D Dual-SLIP model is a hybrid system, switching between single support (SS) and double support (DS) dynamics. During the SS phase, the following dynamics govern the motion of the system

$$\begin{split} m\ddot{p}_{c} &= F_{s,i} + mg \\ m_{f,i}\ddot{p}_{f,i} &= F_{g,i}\hat{z} - F_{s,i} + m_{f,i}g \\ F_{s,i} &= k_{i}(l_{0} - ||l_{i}||)\hat{l}_{i} \\ F_{g,i} &= k_{g,i}(-z_{f,i})^{h} - b_{g,i}\dot{z}_{f,i}(z_{f,i})^{h} \end{split} \tag{1}$$

while during the DS phase, the motion of the system is governed by the following slightly different dynamics

$$\begin{split} m\ddot{p}_{c} &= F_{s,A} + F_{s,B} + m\mathbf{g} \\ m_{f,A}\ddot{p}_{f,A} &= F_{g,A}\hat{z} - F_{s,A} + m_{f,A}\mathbf{g} \\ m_{f,B}\ddot{p}_{f,B} &= F_{g,B}\hat{z} - F_{s,B} + m_{f,B}\mathbf{g} \end{split} \tag{2}$$

where $F_{s,i}$ is the spring force from leg $i \in \{A, B\}$, $\ddot{p}_{f,i}$ is the acceleration of each foot mass, \hat{l}_i is the unit vector along the leg in support i, $g = \begin{bmatrix} 0 & 0 & -9.81 \end{bmatrix}^{\top} \in \mathbb{R}^3$ is the gravity acceleration

²Although the extended model and the proposed controller were first introduced in Ref. [39], certain sections presenting the model are revisited to allow for a more detailed and complete analysis of the proposed framework in this work. Moreover, this work builds upon the previous work of Ref. [39] and introduces an energy-based framework for the tuning of the proposed controller, compares the GRF responses between the model and humans over compliant terrain, and evaluates the system on repeated unilateral low-stiffness perturbations.

³Note that the forward touchdown angle is defined here slightly different than that in Ref. [21].

vector, and $k_{g,i} > 0$ and $b_{g,i} > 0$ denote the stiffness and damping parameters of the ground underneath each leg, and h is equal to 1.5 for a Hertzian nonadhesive contact. The damping parameter of the ground is considered a function of the stiffness

$$b_{g,i} = 1.5c_a k_{g,i} \tag{3}$$

where c_a is constant and equal to 0.2, as in Ref. [15].

As in Ref. [39], the walking steps of the 3D Dual-SLIP model are described by consecutive Midstance (MS) gait events, taking place during the SS phase when $\dot{z}_c = 0$. As the swing leg comes in contact with the ground at Touchdown (TD), the system switches to DS dynamics. The minimum vertical position of the CoM is attained at Lowest Height (LH), while the system switches back to SS dynamics at Lift Off (LO), when the leg in support leaves the ground. Note here that the subsequent MS events correspond to different legs providing support.

2.1.1 Periodic Gaits and Linear-Quadratic Regulator (LQR) Controller. In this work, we utilize a nonlinear optimization technique to derive appropriate values for both the state and control variables, resulting in periodic, left-right symmetric walking patterns. Let x be a slice of the full 3D Dual-SLIP state derived at the MS event, and u be the discrete control input to the system, respectively

$$\mathbf{x} = \begin{bmatrix} x_c - x_{f,i} & y_c - y_{f,i} & z_c & \dot{x}_c & \dot{y}_c \end{bmatrix}^\top, \mathbf{u} = \begin{bmatrix} \theta & \phi & k \end{bmatrix}^\top, \quad k = k_A = k_B$$
(4)

with $i \in \{A, B\}$ again denoting the supporting leg, and the rest of the quantities following the same definition as in Sec. 2.1.

With x_n and u_n denoting the state and control variables at the n-th MS event, the state at the following MS gait event can be calculated as $x_{n+1} = f(x_n, u_n)$, where the mapping f is computed numerically by integrating the hybrid dynamics of the 3D Dual-SLIP model in accord with the sequence of the MS, TD, LH, and LO events. In order to achieve periodic and left-right symmetric walking gaits, where nominally $x_{n+1} = Ax_n$, with A = diag(1, -1, 1, 1, -1), a quarter-period (MS to LH) nonlinear optimization method is adopted to determine a suitable set of state and control variables [21]. Specifically, the optimization's goal is to guarantee that the CoM projection on the ground during the LH event is positioned precisely between the two supporting feet. In turn, this can be accomplished by minimizing the following index

$$\min_{\mathbf{u}_{0}, z_{0}} \left\{ \left\| \frac{1}{2} (x_{f,A} + x_{f,B}(\mathbf{x}_{0}, \mathbf{u}_{0})) - x_{c}(t_{\text{LH}}; \mathbf{x}_{0}, \mathbf{u}_{0}) \right\|^{2} + \left\| \frac{1}{2} (y_{f,A} + y_{f,B}(\mathbf{x}_{0}, \mathbf{u}_{0})) - y_{c}(t_{\text{LH}}; \mathbf{x}_{0}, \mathbf{u}_{0}) \right\|^{2} \right\}$$
(5)

where the system is initiated at MS, t_{LH} denotes the first LH time instance, and x_0 , u_0 represent the initial MS state and control input variables, respectively. Similar to Ref. [21], the optimization search for x_0 is constrained to the following family of states

$$\mathbf{x}_0 = \begin{bmatrix} x_{0,d} & y_{0,d} & z_0 & \dot{x}_{0,d} & \dot{y}_{0,d} \end{bmatrix},$$

s.t. $x_{0,d} = 0$ m, $y_{0,d} = 0.05$ m, $\dot{y}_{0,d} = 0$ m/s

where the forward velocity $\dot{x}_{0,d}$ at MS is selected by the user, while the optimizer specifies values for z_o and the input variables u_0 to minimize the cost function (5). Therefore, for a selected forward velocity, the half-step optimizer identifies a optimal set of initial MS state and control input variables x_0 , u_0 , which ensure that the ground projection of the CoM will be located right in between the two feet in support at the LH event, and by extension lead to a periodic, left-right symmetric walking gait.

The aforementioned methodology was implemented for a forward velocity of 1 m/s and the model parameters shown in

Table 1 Model parameters of the 3D Dual-SLIP model on compliant terrain

Parameter	Value	Units		
Point mass (m)	80	kg		
Foot masses $(m_{f,A/B})$	1	kg		
Leg rest length (l_0)	1	m		

Table 1, and the following optimal set of parameters was obtained through the nonlinear least-squares function *lsqnonlin* in MATLABTM

$$\mathbf{x}_0 = \begin{bmatrix} x_{0,d} & y_{0,d} & z_0 & \dot{x}_{0,d} & \dot{y}_{0,d} \end{bmatrix}$$

= $\begin{bmatrix} 0 \text{ m} & 0.05 \text{ m} & 0.99 \text{ m} & 1 \text{ m/s} & 0 \text{ m/s} \end{bmatrix}$ (7)

$$\mathbf{u}_0 = \begin{bmatrix} \theta_0 & \phi_0 & k_0 \end{bmatrix}^{\mathsf{T}}$$

= $\begin{bmatrix} 107.26 \text{ deg} & 10.94 \text{ deg} & 14163.54 \text{ N/m} \end{bmatrix}$ (8)

Under nominal conditions, an obtained optimal set of parameters x_0^*, u_0^* would result in a periodic left-right symmetric gait, where $x_n^* = A^n x_0^*$, given that the control parameters are chosen so that $u_n^* = B^n u_0^*$ with B = diag(-1, 1, 1) to capture the alternating sign of the forward touchdown angle in every step. However, in nonnominal conditions under the influence of disturbances $x_n \neq x_n^*$, where x_n represents the *actual* value of the state at the *n*-th MS event, meaning that the system will not achieve the desired periodic gait. To tackle this issue and guarantee that x_n will approach the desired periodic behavior, an identity discrete-time, infinite-horizon LQR controller is employed, described by the following control law

$$\boldsymbol{u}_n = \boldsymbol{u}_n^* + \boldsymbol{B}^n \boldsymbol{K} \boldsymbol{A}^n (\boldsymbol{x}_n - \boldsymbol{x}_n^*) \tag{9}$$

which regulates the control input in every MS event to ensure that the state converges to the desired periodic gait⁴.

Although the half-step optimization analyzed earlier is not valid for uneven terrains [23], it can be utilized for surfaces with high ground stiffness values. As a validation of the modified dynamics and the methodology for achieving periodic gaits, rigid terrain was simulated first by testing locomotion over a surface with a high ground stiffness of $k_{g,A}=k_{g,B}=50~\mathrm{MN/m}$ [39]. For all simulations, the optimal parameter values found in (7)–(8) and the identity LQR controller (9) were used, while the corresponding model parameters are listed in Table 1. The system response is shown in Fig. 2, where although more than 100 steps were achieved, for brevity only the system response up to the 25th step is shown. Moreover, during locomotion over this ground stiffness, the vertical GRF response for each leg ($F_{g,A}$ and $F_{g,B}$) exhibits the characteristic double-peaked shape observed in human walking [20], as illustrated in Fig. 3.

2.1.2 Energy Conservation and Error Tolerance. As shown in Sec. 2.1, the 3D Dual-SLIP model is unactuated, and hence no energy can be injected into or removed from the system. Specifically, among the control inputs, only the leg stiffness k_i is associated with the energy of the system, as shown by the following equation:

$$E_{\rm MS} = \frac{1}{2}m||\dot{\boldsymbol{p}}_c||^2 + \frac{1}{2}k_i(l_0 - ||\boldsymbol{l}_i||)^2 + mgz_c$$
 (10)

where E_{MS} is the total energy of the system at the MS event. It can be seen from (10) that the total energy at MS is affected by the leg stiffness k_i both directly, through the spring energy, and indirectly, through the displacement z_c of the mass and its velocity \dot{p}_c . We computed the sensitivity $\frac{\partial E_{MS}}{\partial k}$ of the total energy at MS with respect

⁴For the full derivation of the time-invariant feedback gain *K* of the identity LQR controller the reader is referred to Ref. [39].

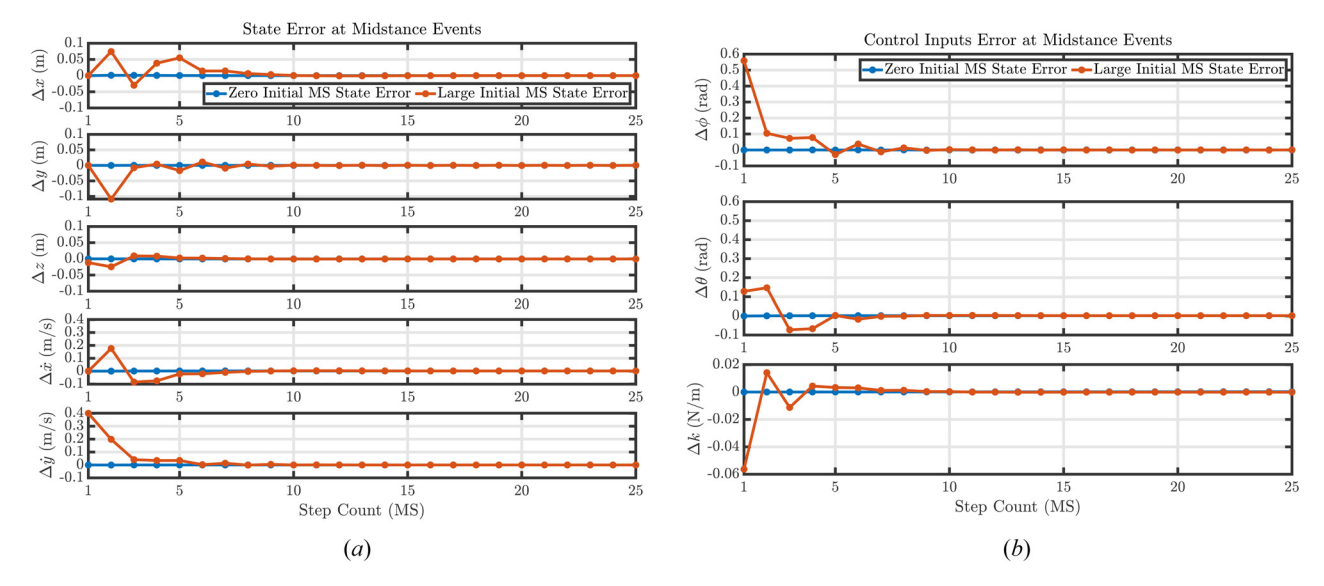


Fig. 2 State (a) and control (b) input error response with zero and with a large initial MS state error ($\Delta z(1) = -0.0118$ m, $\Delta \dot{y}(1) = 0.4$ m/s) using the LQR controller

to the leg stiffness numerically and we found it to be significant: $0.7020\,\mathrm{m}^2$. However, the sensitivity $\left|\left|\frac{\partial f}{\partial k}\right|\right|$ of the return map with respect to the leg stiffness was found to be low, namely, 0.0049. As a result, this prevents the LQR controller from applying significant changes in leg stiffness, hence rendering the leg stiffness value practically constant during walking.

Regarding energy losses for the system, it should be noted that all contacts are assumed to be frictionless in the 3D Dual-SLIP model, while for a sufficiently small foot mass $(m_{f,i} \ll m)$, its total energy can be assumed to be negligible compared to the total energy of the system. However, there are energy losses during locomotion due to the damping properties of the ground. Naturally, the magnitude of the energy losses depends on the damping of the terrain, which in the scope of this work has been assumed to be linearly dependent on the ground stiffness, as (3) indicates. For extremely high ground stiffness values, despite the corresponding high damping, energy losses are minimal, for the excessive interaction forces $F_{g,A/B}$ constrain the vertical movement of the foot masses $(\hat{z}_{f,A/B} \to 0)$. For instance, for walking on rigid terrain $(k_{g,A/B} = 50 \text{ MN/m})$ using the optimal parameters values (7)–(8), an identity LQR controller, and the model parameters of Table 1, the system is losing energy at quite

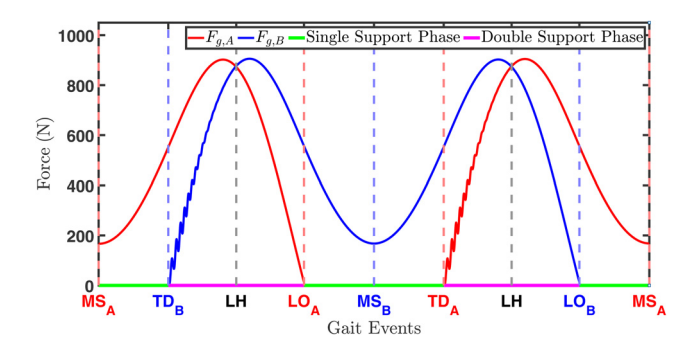


Fig. 3 Response of the vertical GRF for each leg during two steps over a rigid ground stiffness (50kN/m). Red and blue lines correspond to the vertical GRFs $F_{g,A}$ and $F_{g,B}$ applied at the feet of leg A and B, respectively. Solid green and magenta horizontal lines on the horizontal axis of the figure indicate the duration of the SS and DS phases, respectively. Dashed vertical red and blue lines denote the time instances of the MS, TD, and LO gait events associated with the leg A and B, respectively, while black lines denote the time instances of the LH gait events. The subscripts of the MS, TD, and LO gait events represent the associated leg.

a small rate (0.0028 J per step). Therefore, it can be assumed that the total energy of the system is practically conserved during locomotion over rigid surfaces.

The initial total energy of the system is determined by the model parameters and the utilized set of optimal gait parameters x_0^* , u_0^* . As a consequence, during locomotion over rigid surfaces, each optimal set of gait parameters can be associated with a specific value for the conserved total energy of the system. For the optimal parameters of (7)–(8) and the model parameters of Table 1, the initial total energy is equal to $E_{MS_0} = 815.9032 \ J$.

In order to explore the robustness of the LQR controller presented in the previous subsection, we investigated the influence of applying disturbances on the initial MS state of the system x_0^* . As it was explained above, by adjusting the initial MS state, the initial total energy of the system is generally modified. Therefore, if the system converges, it will do so at a set of MS states and control inputs that correspond to the modified total energy level. As a result, for disturbed initial conditions that lead to an initial total energy different than the undisturbed one (E_{MS_0}) , a steady-state error will be observed. This is true because the utilized identity LQR controller was designed specifically for the undisturbed set of optimal gait parameters x_0^*, u_0^* . As expected, due to the fact that the return map sensitivity to leg stiffness is extremely low, the LQR controller utilized practically the same leg stiffness throughout the experiment⁵. This intuitively explains why the LQR controller is unable to bring the system back to its nominal total energy, thereby leading to a nonzero steady-state error.

Based on the above, we focused only on perturbed initial MS states that correspond to a total energy equal to the one for the unperturbed case ($E_{\rm MS_0}$). As shown in Fig. 2, with the LQR controller, the regular 3D Dual-SLIP model can tolerate relatively large MS state errors. Specifically, the system was able to handle deviations up to $0.4\,\mathrm{m/s}$ from the desired lateral velocity \dot{y}_0 , while an error of $-0.0118\,\mathrm{m}$ was applied to the initial vertical position z_0 to maintain the initial total energy equal to its unperturbed value $E_{\mathrm{MS_0}}$. Therefore, it is shown that by exploiting the energy conservation of the model, the unactuated 3D Dual-SLIP model is able to tolerate relatively large MS state errors. This is of high importance, as Liu et al. had implied that only the actuated 3D Dual-SLIP model was able to handle disturbances of that magnitude [44]. As a result, the importance of energy conservation in the error

 $^{^5}$ For a 100-step simulation using the parameters of (7)–(8), an identity LQR controller, and the model parameters of Table 1, a sensitivity of $||\frac{\partial^2}{\partial t}|| = 0.0049$ and an average leg stiffness of $14163.54 \pm 2.58 \times 10^{-4} N/m$ were found.

tolerance of the unactuated 3D Dual-SLIP model is highlighted here, which has been unexplored by previous works, including that of Liu (2015). Recall that Fig. 2 depicts only the first 25 steps for brevity, although the system was able to achieve more than 100 steps, indicating stable performance [20].

2.2 Bio-Inspired Proposed Controller. The response of the 3D Dual-SLIP model to one-step unilateral low ground-stiffness perturbations was recently investigated, aiming to achieve periodic gait over compliant surfaces [39]. In brief, after identifying a set of optimal gait parameters for achieving periodic gait, the locomotion of the model was simulated over rigid terrain (50 MN/m). At the n_p step of the model, a one-step unilateral low ground-stiffness perturbation was induced in the system, while the ground stiffness returned to rigid after the completion of the step. Similar perturbations have been induced previously in humans for gait rehabilitation and for understanding human locomotion using a novel instrumented device [45–47].

To handle such perturbations, a bio-inspired controller was recently proposed that adjusts the leg stiffness values of the 3D Dual-SLIP model, mimicking the same behavior observed in humans [39]. In more detail, biomechanics research shows that humans and birds adjust the stiffness of their legs based on ground stiffness [35–38]. Specifically, Ferris et al. showed that the stiffness of both legs increases for runners during their first step when transitioning from a hard to a softer surface [37]. Moreover, as the transition between surfaces is expected, a tendency to pre-adjust the increased leg stiffness is observed during the final step of the runners on the hard surface. Mimicking this behavior, the recently proposed bioinspired controller increased the stiffness of the legs in the 3D Dual-SLIP model, managing to achieve robust dynamic walking over ground-stiffnesses as low as $30 \, \text{kN/m}$ [39].

The bio-inspired controller is a modified version of the LQR controller mentioned in (9), which allows the adjustment of the stiffness in the legs of the 3D Dual-SLIP model when necessary (Fig. 4). As a reminder, the LQR controller consists of the following control law: $\mathbf{u}_n = [\theta_n \quad \phi_n \quad k_n]^\top = \mathbf{u}_n^* + \mathbf{B}^n \mathbf{K} \mathbf{A}^n (\mathbf{x}_n - \mathbf{x}_n^*)$, which adjusts the control input \mathbf{u}_n at the MS event of each step n, guaranteeing convergence of the state \mathbf{x}_n to the desired periodic gait characterized by the nominal state \mathbf{x}_n^* and control input \mathbf{u}_n^* .

In more detail, initially—before the perturbation is encountered—at every step n the LQR controller derives a leg stiffness value k_n as part of the control input u_n , which is shared by both legs $(k_A = k_B = k_n)$. When the TD event takes place during the perturbation step n_p , the stiffness of the leg about to touch the ground is amplified to $k_A = k_1 k_{n_p}$, where $k_1 > 1$ represents a control gain and k_{n_p} is the leg stiffness value determined by the LQR controller. Similarly, the stiffness of the other leg (already in support) is also amplified to $k_B = k_2 k_{n_p}$, where $k_2 > 1$ is also a separate control gain. When the MS event of the next step $(n_p + 1)$ takes place, the stiffness

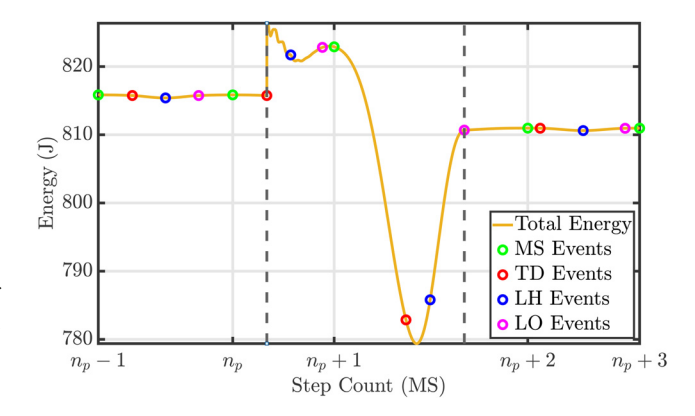


Fig. 5 Response of the total energy of the system for a ground stiffness perturbation of $30 \, kN/m$ induced at step $n_p = 10$ using the control gains $k_1 = 6$ and $k_2 = 2$ for the proposed controller

of the leg about to touch down on a rigid surface is set back to $k_B = k_{n_p+1}$, while the stiffness of the perturbed leg maintains the same control gain $k_A = k_1 k_{n_p+1}$. When the following MS event happens, the perturbed leg will be in swing phase (LO) and about to touch down on a rigid surface. As a result, for every step $n > n_p + 1$, the LQR controller will be again determining the shared stiffness of both legs k_n . The 3D Dual-SLIP model together with the bio-inspired controller constitute an actuated system, which allows adjusting rapidly the leg stiffness values of the model. However, it is not necessary for a bipedal robot to adjust the stiffness of its legs, in order to track desired trajectories generated by this actuated system.

To understand the effect of the proposed controller on the total energy of the system during a one-step unilateral ground-stiffness perturbation, consider, as a representative example, the total energy response for a ground stiffness perturbation of $30 \, kN/m$ induced at step $n_p = 10$ shown in Fig. 5. It can be seen that before the perturbation step (n_p) , the 3D Dual-SLIP model walks on rigid stiffness terrain with its total energy being practically conserved, as was expected from Sec. 2.1.2. When the TD event takes place during the perturbation step, the control gains k_1 , k_2 are applied, resulting in the amplified leg stiffness values $k_A = k_1 k_{n_n}$ and $k_B = k_2 k_{n_n}$. As the leg in support continues to compress at TD, energy is injected into the system by amplifying the leg's stiffness. In contrast, amplifying the stiffness of the leg that has just touched the ground is not injecting energy, as its length is equal to the rest length at TD. Moreover, at that point the ground stiffness perturbation takes place and the foot of the perturbed leg starts "sinking" into the ground, leading to significant energy loss due to the damping of the ground. When the MS event of the $n_p + 1$ step happens, the leg that is experiencing the perturbation, now in support, retains the same amplified stiffness, while the stiffness of the leg about to touch down

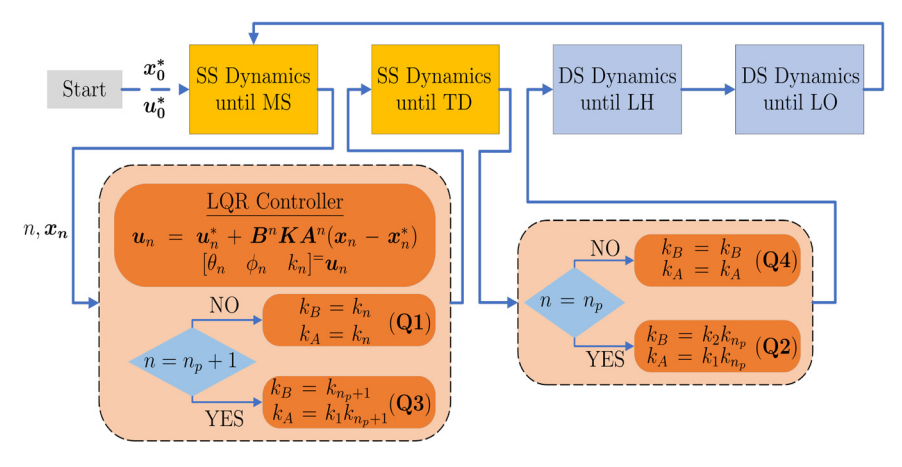


Fig. 4 Outline of the bio-inspired controller proposed in Ref. [39]

on a rigid surface is decreased to $k_B = k_{n_p+1}$. This decrease in leg stiffness does not remove energy from the system, as it takes effect at the next TD event, where the corresponding leg is at rest length. At the LO event of the n_p+1 step, the stiffness perturbation has been completed, hence from that point on the total energy of the system is again conserved, as it was before the perturbation. Finally, at the MS event of the n_p+2 step, the perturbed leg has its stiffness also decreased back to $k_A=k_{n_p+2}$, where again the total energy of the system is not affected.

Therefore, during a ground stiffness perturbation, the system initially gains some energy due to the amplified leg stiffness and then loses some energy due to the compliant nature of the terrain, at a rate that depends on both the damping of the terrain and the control gains of the proposed controller. As a result, the new conserved value of the total energy after the ground stiffness perturbation depends on its magnitude and on the control gains of the proposed controller.

3 Results

In this section, the tuning of the proposed controller is analyzed, the GRF response of the model is compared to the one observed in humans, and the performance of the proposed controller is evaluated under repeated unilateral low-stiffness perturbations. Similar to previous sections, for all simulations the optimal parameter values found in (7)–(8) and an identity LQR controller were used, while the corresponding model parameters are listed in Table 1. All one-step unilateral low ground-stiffness perturbations took place at the tenth step ($n_p = 10$). All the processing and the simulations were completed in MATLABTM version 9.7 (R2019b), using the nonlinear least-squares function lsqnonlin and the embedded variable step integrator ode4.

3.1 Control Gains Tuning for the Proposed Controller. Previously in Ref. [39], it was stated that the control gains of the proposed controller can be tuned for a specific stiffness perturbation so that the steady-state error is minimized. However, as mentioned in Sec. 2.1.2, the steady-state error response of the system is associated with the total energy of the system, which is conserved. As shown in Sec. 2.2, the conserved total energy of the system after the ground stiffness perturbation is affected significantly by the control gains of the proposed controller. Therefore, to analyze how the gains k_1 and k_2 of the proposed controller can be tuned for a specific stiffness perturbation, their relationship with the total energy of the system is investigated here.

In order to minimize the steady-state error for the state response, it is necessary for the system to have the same total energy before and after the perturbation. Therefore, the steady-state error can be minimized by identifying a set of control gains for the proposed controller that will lead to a nearly zero total energy difference before and after the perturbation. For this purpose, an exhaustive grid search was performed across a range of control gains for different ground stiffness perturbations. For this analysis, the total energy difference was defined as follows:

$$\Delta E = E_{\text{MS}_{n_p+2}} - E_{\text{MS}_{n_p}} \tag{11}$$

where $E_{\mathrm{MS}_{n_p}}$ and $E_{\mathrm{MS}_{n_p+2}}$ are the total energies of the system at the MS events of steps n_p and n_p+2 , respectively. Three representative examples of such exhaustive grid searches for ground stiffness perturbations of 30, 60, and 90 kN/m are shown in Fig. 6. As it can be seen, for every control gain combination that leads to a total of 100 successful steps, either a negative or a positive ΔE will be achieved. Moreover, combinations belonging to each category seem to form two distinct clusters, noted as green ($\Delta E > 0$) and red ($\Delta E < 0$) areas in Fig. 6. Therefore, the combinations of interest with $\Delta E = 0$ lie at the borders between those two clusters. Furthermore, as the ground stiffness receives lower values, the size of the positive ΔE (green) cluster, initially increases ($60 \, kN/m$), and then it decreases significantly for extremely low-stiffness values ($30 \, kN/m$). A similar trend is observed for the number of control

gain combinations that lead to $\Delta E = 0$, and by extension to zero steady-state error. Moreover, as ground stiffness decreases, in general, higher control gains are required to achieve 100 steps. It should be noted that these are extremely low-stiffness values that result in an excessive vertical penetration of the leg experiencing the perturbation into the ground that exceeds 10 cm (10% of the model's leg length at rest) for the lowest ground stiffness of $30 \, kN/m$ [39].

For illustration purposes, the total energy evolution of the system for combinations leading to a positive, negative and zero ΔE is presented in Fig. 7(a), for a ground-stiffness perturbation of $90 \, kN/m$. In addition, the corresponding responses of the CoM vertical position z_c and velocity \dot{z}_c in phase space are depicted in Fig. 7(b), where it can be seen that before the perturbation, where the total energy is conserved, the system tracks a cyclic closed trajectory noted in blue line. After the perturbation, it is shown that for positive (orange line), zero (yellow line), and negative (purple line) ΔE , the system converges in steady-state to larger, similar, and smaller cyclic closed trajectories, respectively. Therefore, by selecting control gains that lead to $\Delta E = 0$, the system can converge after the perturbation back to the initial tracked closed trajectory, hence driving the steady-state error to zero.

It can be seen in Fig. 6 that multiple combinations of gains exist that satisfy the $\Delta E = 0$ condition. For that reason, for each ground stiffness perturbation, an optimal set of control gains is defined as the combination that satisfies the energy condition with the lowest possible control gains. This choice would minimize control effort in a real robot implementation. As shown in Ref. [39], for the model and optimal parameters utilized for this work, the proposed controller is employed only when the ground stiffness is lower or equal to $200 \, kN/m$, as for higher values the standard LQR controller would suffice ($k_1 = k_2 = 1$). For that reason, optimal control gains were identified only for stiffness values lower or equal to $200 \, kN/m$. The optimal control gains identified for stiffness values up to $30 \, kN/m$ are illustrated in Fig. 8, while a nonlinear curve fitting was applied for each control gain using a nonlinear least-squares algorithm. Specifically, the following nonlinear curve was fitted to the data

$$k_w^f(k_g) = c_1 e^{-c_2 k_g} - c_3 \ln(c_4 k_g)$$
 (12)

where $w \in \{1,2\}$, and $c_1,c_2,c_3,c_4 \in \mathbb{R}$ are the four parameters to be tuned for each fitted curve, k_1^f and k_2^f . As shown in Fig. 8, both control gains increase exponentially as the perturbation ground stiffness decreases, while they converge to 1 for ground stiffness values higher than $200 \, kN/m$. Moreover, the decaying exponential-logarithmic curve fitting matches quite accurately the identified combinations, hence providing a convenient and precise way of identifying optimal control gains for any kind of ground stiffness perturbation. The tuned parameters for the nonlinear curve fitting for each control gain are reported in Table 2. It should be noted that the tuned gain parameters are specific to the employed optimal gait parameter values (x_0, u_0) and model parameters reported in (7)–(8) and Table 1, respectively. Therefore, the fitting process, as well as the identification of the control gains of the proposed controller across different ground stiffness values using (12), would need to be repeated for different model variations or baseline gaits.

3.2 Comparison of Ground Reaction Force Profiles Between Humans and the 3D Dual-Spring-Loaded Inverted Pendulum Model. As mentioned in the introduction, the 3D Dual-SLIP model has been established as an accurate model of human walking, as it produces human-like CoM vertical oscillations and lateral sway, as well as vertical GRF responses. However, these findings have only been verified for locomotion over rigid terrain [20,21]. In order to explore how accurately the 3D Dual-SLIP model captures human walking over compliant terrain, the vertical GRF responses of a human and the model during a one-step unilateral low ground-stiffness perturbation are compared.

Specifically, a healthy human subject (age: 25, height: $1.91 \, m$, weight: $87.59 \, kg$) was asked to walk on a unique robotic device, the

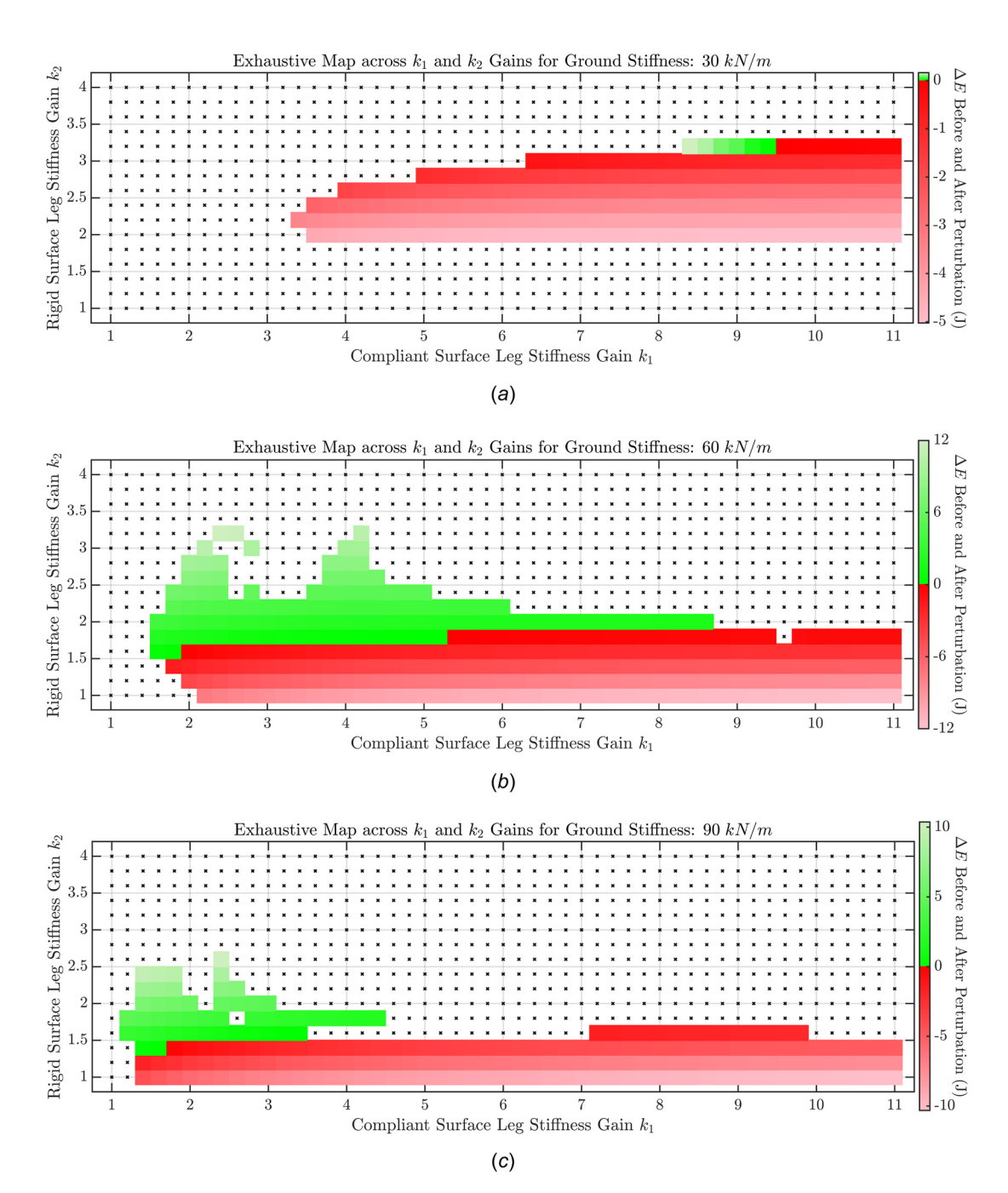
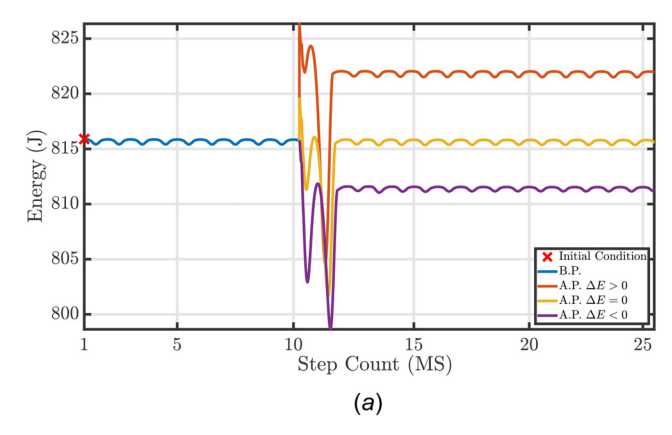


Fig. 6 Representative examples of exhaustive grid searches across a wide range of control gains for ground stiffness perturbations of $30 \, kN/m$ (a), $60 \, kN/m$ (b), and $90 \, kN/m$ (c). Horizontal and vertical axes correspond to the control gains applied on the stiffness of the legs stepping on the compliant (k_A) and the rigid (k_B) surface, respectively. Green and red nodes correspond to control gain combinations that achieved 100 steps and led to positive and negative changes in total energy ΔE before and after the perturbation, respectively, while black crosses (\times) indicate combinations that failed to achieve 100 steps. Shade of colored nodes illustrates the magnitude of the energy change; paler combinations are associated with larger energy changes.

Variable Stiffness Treadmill (VST) [47,48]. The VST has been used in numerous studies for understanding the human gait on compliant terrain [49–55]. In short, the VST is a split-belt treadmill that allows for repeatable unilateral stiffness perturbations, by dynamically decreasing the vertical ground stiffness of the left belt, while humans walk on it. For our experiment here, the subject walked at a speed of 1 m/s for 20 consecutive gait cycles over rigid terrain (1 MN/m) and then experienced 10 consecutive one-step unilateral ground-stiffness perturbations of 90 kN/m under the left leg. The vertical GRF response under the subject's left leg was recorded at 60 Hz using a force sensor map (Medical Sensor 3150^{TM} , Tekscan, Inc., South Boston, MA) placed underneath the left belt of the treadmill.

The recorded GRF data were filtered with a 4th-order zero-phase Butterworth filter (cutoff at $4\,Hz$). For the vertical GRF responses of the 3D Dual-SLIP model, the model was simulated walking at $1\,m/s$ over rigid terrain $(50\,MN/m)$ and experiencing one-step unilateral ground-stiffness perturbations at $90\,kN/m$ after ten steps over rigid terrain. Three different simulations were conducted for the stiffness perturbations, where in each one the proposed controller was utilized with control gains $k_1=1.4$ and $k_2=1$, $k_2=1.36$, and $k_2=2$, leading to $\Delta E<0$, $\Delta E=0$, and $\Delta E>0$, respectively. The average recorded human and simulated model GRF responses during the stance phase for all conditions are shown in Fig. 9.



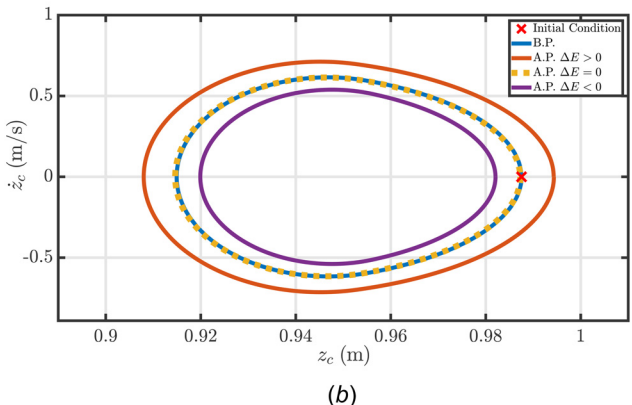


Fig. 7 Representative examples of total energy (a) and phase space (b) response (z_c versus z_c) of the model for control gains that lead to $\Delta E > 0$, $\Delta E = 0$ and $\Delta E < 0$. For this example, the system was simulated using a stiffness perturbation of 90~kN/m at $n_p = 10$ with control gains $k_1 = 1.4$ and $k_2 = 2$, $k_2 = 1.36$, and $k_2 = 1$, for the $\Delta E > 0$, $\Delta E = 0$ and $\Delta E < 0$ cases, respectively. Blue lines represent the system response before the perturbation (B.P.), while orange, yellow and purple lines depict the system response after the perturbation (A.P.) in steady-state for a positive, zero, and negative ΔE , respectively. The red cross (×) indicates the initial condition of the system.

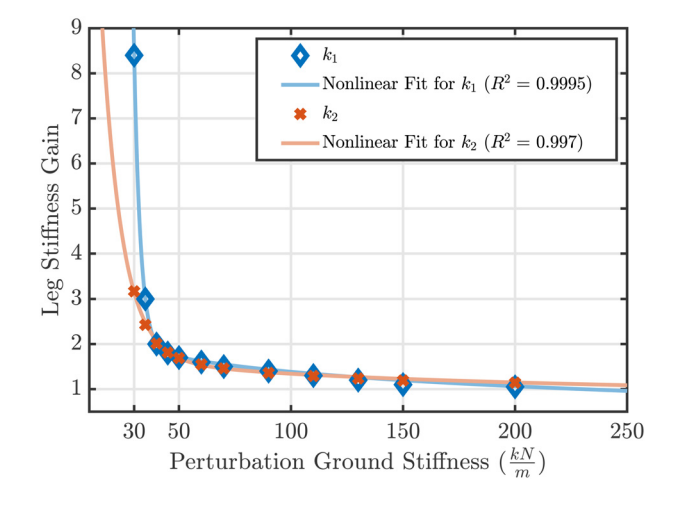


Fig. 8 Optimal control gains of the proposed controller with respect to the perturbation ground stiffness. Blue diamonds (\diamondsuit) and orange crosses (\times) represent the identified optimal control gains for the stiffness of the leg stepping on compliant (k_1) and rigid (k_2) surfaces, respectively, while blue and orange solid lines denote the corresponding fitted nonlinear curves. The corresponding coefficients of determination R^2 for each fitted curve are reported in the legend of the figure.

Table 2 Derived parameters for the nonlinear curve fitting applied to the optimal control gains shown in Fig. 8

	c_1	c_2	c_3	c_4
k_1^f	227310	0.3488	0.4622	0.0005
k_2^f	41.4691	0.1112	0.2777	0.00008

As can be seen, the human and model responses are quite similar to each other for both conditions, i.e., rigid and compliant terrain. Specifically, for walking over rigid terrain, similarly to Fig. 3, the model again matches the characteristic double-peaked shape also exhibited by the human subject, which is typically observed in human walking [20,37,56]. For the one-step unilateral stiffness perturbations, in the human subject case, the GRF response agrees with [37], where the first peak and the valley of the GRF seem to be lower in magnitude compared to the rigid terrain, while the second peak seems to be higher. Moreover, both the peaks and the valley appear to take place at later stance phase percentages, again compared to the rigid ground response. Similarly, for all three variations of the proposed controller, the 3D Dual-SLIP model also exhibits a lower magnitude for the first peak, which becomes more evident for control gains with larger ΔE . In contrast, the magnitude of the second peak seems to increase for control gains with larger ΔE , while it stays similar to rigid ground levels for $\Delta E = 0$. Regarding the valley, it appears to be higher in magnitude for all three control gains compared to the rigid ground level, while control gains with larger ΔE appear to lead to smaller increments. Lastly, both the peaks and the valley appear to occur earlier in the stance phase for compliant terrain, which seems to become more evident with control gains that cause larger ΔE . Therefore, in general, the 3D Dual-SLIP model appears to behave in a qualitatively similar fashion with humans during locomotion over compliant terrain, while control gains with $\Delta E > 0$ seem to produce more human-like GRF responses, in terms of the magnitude of the two peaks and the valleys. It should be noted that modeling accurately human walking over rigid and compliant terrain is not the goal of this work. The qualitative comparison above was only performed to gain some intuition regarding the similarity of the extended model to human behavior over compliant terrain.

3.3 Repeated Unilateral Stiffness Perturbations. So far, the behavior of the system to a single one-step unilateral ground-stiffness perturbation has been analyzed. However, as we are interested in biped locomotion over compliant surfaces, the performance of the proposed controller over repeated unilateral stiffness perturbations needs to be investigated.

In order to explore whether the proposed controller can handle consecutive one-step unilateral stiffness perturbations, the minimum number of steps n over rigid terrain between two such perturbations will be identified, for different pairs of various ground stiffness values. Specifically, for these simulations, the system was first initialized and walked over rigid terrain for $n_p - 1$ steps, and then it experienced a one-step unilateral perturbation of ground stiffness s_1 , exactly as described in Sec. 2.2. After that, the system walked again over rigid terrain for n steps, and then experienced again a one-step unilateral perturbation of ground stiffness s_2 , followed by locomotion over rigid terrain until either failing or reaching a total of 100 steps. An overview of the above procedure is depicted in Fig. 10. For each perturbation, the control gains of the proposed controller were tuned to maintain $\Delta E = 0$, as discussed in Sec. 3.1. The minimum number of steps *n* required for achieving 100 steps for all pair combinations (s_1 - s_2) across five ground stiffness values of 200, 150, 110, 70 and 30 kN/m are reported in Table 3. As it can be seen, two steps with the perturbed leg over rigid terrain (corresponding to five total steps) are necessary for the system to handle most cases of successive perturbations, while in some cases as in when $s_2 = 30 \text{ kN/m}$, only one step with the perturbed leg (corresponding to three total steps) are required. Therefore, it is clear

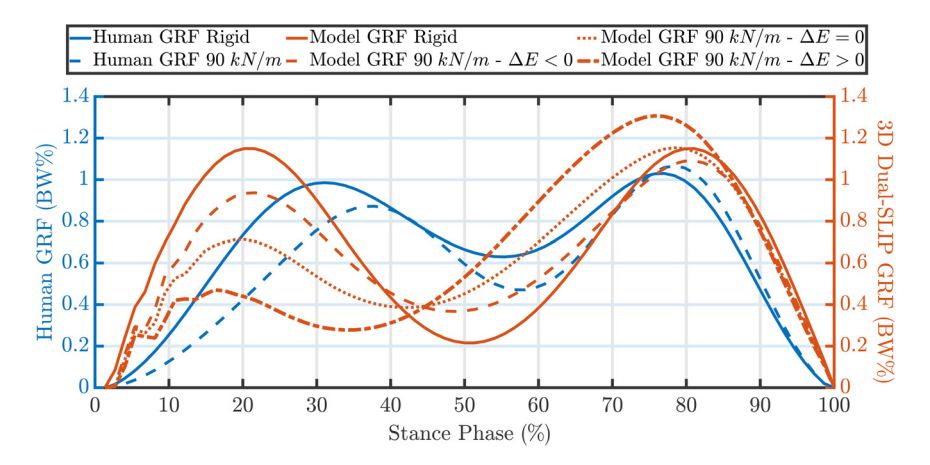


Fig. 9 Comparison between the vertical GRF responses observed in the 3D Dual-SLIP model and a human on rigid and compliant surfaces. Blue solid and dashed lines correspond to the average human vertical GRF responses during a step over rigid and a one-step unilateral ground-stiffness perturbation at 90 kN/m, respectively. The orange solid line denotes the 3D Dual-SLIP vertical GRF response for a step over rigid terrain, while orange dashed, dotted and dash-dotted lines illustrate the model vertical GRF response during stepping on terrain with stiffness of 90 kN/m using control gains leading to $\Delta E < 0, \Delta E = 0,$ and $\Delta E > 0,$ respectively. The left and right vertical axes represent the human and model GRF as a percentage of body weight (BW). The horizontal axis represents time as a percentage of the stance phase.

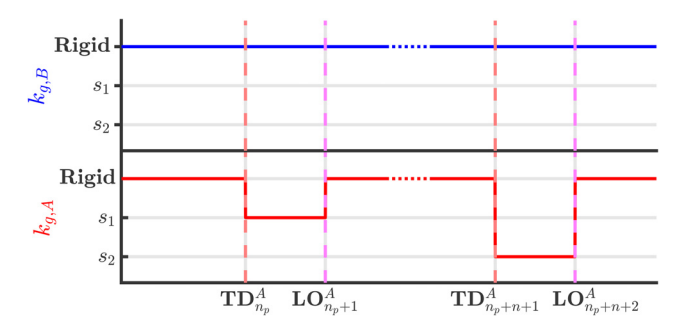


Fig. 10 Outline of the two one-step unilateral low ground-stiffness perturbations. Top and bottom figures present the ground stiffness levels under the legs B and A, respectively. A ground stiffness of $50 \, kN/m$ corresponds to rigid terrain, while the ground stiffness values s_1 and s_2 are selected to test all pair combinations across the five ground stiffness values of 200, 150, 110, 70 and 30 kN/m. Superscript and subscript in each gait event indicate the corresponding leg (A or B) and the step number, respectively.

that the passive nature of the proposed system and controller allows for repeated stiffness perturbations only if a minimum number of steps with the perturbed leg (2 or 1) on rigid surface are introduced in between the two compliant surface perturbations. A further discussion on this follows below. Additionally, it should be

Table 3 Required minimum number of total and perturbed-side (in parenthesis) steps between two one-step unilateral low-stiffness perturbations for achieving steady-state. For all pair combinations, a total number of at least 100 steps was achieved

				s ₂ kN/m		
		200	150	110	70	30
	200	5(2)	5(2)	5(2)	5(2)	3(1)
	150	5(2)	5(2)	5(2)	5(2)	3(1)
s ₁ kN/m	110	5(2)	5(2)	5(2)	5(2)	3(1)
	70	5(2)	5(2)	5(2)	5(2)	3(1)
	30	5(2)	5(2)	5(2)	5(2)	5(2)

mentioned that in all combinations, although 100 steps were achieved, a steady-state error was observed, which intensified as the perturbation ground stiffness values decreased. This indicates that the total energy difference is nonzero for the second perturbation, despite the tuning of the proposed controller. Although the total energy is immediately stabilized after the first perturbation to its nominal value ($\Delta E = 0$), the LQR controller requires a number of steps to regulate the introduced state error. As a result, if there is a state error when the second perturbation takes place, tuning the proposed controller with the control gains identified in Sec. 3.1, might not lead to $\Delta E = 0$, hence resulting in a steady-state error. It should be noted that perhaps a different set of control gains could be identified to handle two back-to-back repeated perturbations, but this methodology would not generalize for any number of such perturbations. A video demonstrating the 3D Dual-SLIP model experiencing repeated one-step unilateral ground-stiffness perturbations is available at the website address found in the footnote.⁶

4 Discussion

This work presents a new framework for dynamic locomotion of bipeds across very compliant surfaces. Although bipeds have achieved robust locomotion over compliant terrain in previous works [5,6,8–12], there is a need for a general framework applicable to different bipeds that allows for stable locomotion over various compliant terrains. To fill this gap, the 3D Dual-SLIP model was previously modified to support locomotion over compliant terrain for the first time [39]. There, a novel bio-inspired controller was also proposed enabling the adjustment of the stiffness for both legs of the model and it was shown that stable gait after one-step unilateral ground-stiffness perturbations can be achieved, for ground stiffness values as low as $30 \, kN/m$ [39]. In this paper, we extended this work by introducing an energy-based methodology for the systematic tuning of the bio-inspired controller, to allow for dynamic walking with robustness over a wide range of low-stiffness unilateral onestep perturbations. Furthermore, human vertical GRF responses over compliant terrain were recorded and compared to the equivalent GRF responses of the extended 3D Dual-SLIP model, showing that this model in a closed-loop with the proposed controller produces qualitatively human-like responses even over

⁶https://www.youtube.com/watch?v=IfyqaeqL3dc

compliant terrain. Therefore, we anticipate that the proposed framework will be useful in achieving human-like walking with bipedal robots over compliant terrains, as well as modeling human walking over such surfaces. Moreover, the proposed system and controller were shown to be capable of handling repeated unilateral low ground-stiffness perturbations, given that a sufficient number of steps over rigid terrain take place between consecutive perturbations. Lastly, it should be noted that the framework proposed in this work can lead to stable gait over very soft terrains of stiffness down to $30 \, kN/m$, which can result in excessive penetration of the perturbed leg into the ground exceeding 10% of its length at rest.

As shown in the previous subsection, the 3D Dual-SLIP model is able to handle repeated one-step unilateral ground-stiffness perturbations with the bio-inspired controller, as long as they occur every 3(1) to 5(2) steps. In other words, the proposed scheme can not handle perturbations that happen with less than 3 steps in between, even at moderate ground stiffness levels $(200 \, kN/m)$ [15]. As a consequence, transitions from rigid to compliant terrain for both legs cannot be supported as well, hence ruling out the locomotion of the model over compliant terrain. The underlying reasons behind this limitation of the proposed controller will be analyzed below.

First, the proposed controller is based on a standard discrete-time LQR controller that is being invoked discretely only at every MS event. As a result, the control inputs of the model can only be updated once per step. The proposed controller inherits this limiting property, although it allows for the additional adjustment of the leg stiffness control input during the perturbation. This feature restricts significantly the performance of the proposed controller, as it is not reacting fast enough to regulate any introduced state errors, which can destabilize the system.

Secondly, the amount of energy that the proposed controller can inject into the system is limited. In this work, it was shown that in order to minimize steady-state error, the total energy of the model has to remain the same before and after a ground stiffness perturbation, during which considerable energy is lost. As analyzed in Sec. 2.1.2, out of all the control inputs of the model, only the leg stiffness can affect the total energy of the system. However, as shown in Sec. 2.1.2, the LQR controller does not apply significant changes in leg stiffness, while the proposed controller, although capable of adjusting leg stiffness considerably, can act only once per step perturbation. Therefore, when stiffness perturbations are applied at every consecutive touchdown, the proposed controller is unable to inject sufficient energy in time to counteract the energy losses due to the ground damping.

Therefore, it is clear that there is a need for a continuous control input that would be able to regulate significantly the energy of the system whenever necessary. Research in biomechanics has shown that the ankle joint is crucial for propulsion and balance during standing and walking while being one the largest sources of mechanical power during walking [57]. At the same time, rehabilitation research has focused extensively on replicating these effects through lower-limb assistive devices [58]. Hence, by introducing an actuated ankle joint into the model, the system would be able to regulate introduced state errors and balance energy losses rapidly and continuously. Although similar extensions have been proposed in previous works for bipedal models [27,33,59], to the best of our knowledge there has not been such an extension neither for the 3D Dual-SLIP model nor to enable locomotion over compliant terrain. Therefore, future work will explore whether an extended 3D Dual-SLIP model with ankle-actuated finite-sized feet could overcome the aforementioned limitations of the model, and possibly support locomotion over compliant terrain.

Furthermore, it should be noted that this work investigates ground stiffness perturbations under the assumption that they are expected and of known properties. In other words, in order to tune appropriately the control gains of the proposed controller, both the timing and the magnitude of the ground stiffness perturbation have to be known a priori. This limitation could be addressed by estimating the ground stiffness in real-time based on the foot-ground interaction force $F_{g,A/B}$ and states of the system, such as the vertical

positions of the feet $z_{f,A/B}$. Similar schemes have been implemented in previous works on bipeds, for both real robots and simulated models, where ground stiffness was accurately estimated in realtime without introducing significant delays into the system [1,2,60]. In order to highlight the importance of estimating the ground stiffness in real-time, the system's performance in scenarios involving a disparity between expected and actual perturbations is briefly analyzed here. Consider the case where a single one-step unilateral ground-stiffness perturbation of $90 \, kN/m$ is expected, but a significantly lower ground stiffness of $60 \, kN/m$ is encountered. Therefore, this is equivalent to not utilizing the optimal control gains to handle an expected ground-stiffness perturbation. In this case, the proposed controller will lead to a nonzero total energy difference before and after the perturbation ($\Delta E \neq 0$), hence resulting in some steady-state error. However, this does not imply that the system will fail immediately. As shown in Fig. 6, the model is able to achieve 100 steps for various combinations of control gains in the neighborhood of the optimal control gains. Additionally, even for the combinations where 100 steps cannot be achieved (indicated by black crosses in Fig. 6), the model typically continues to walk for a large number of steps. Therefore, the ability to estimate the ground stiffness in real-time would be highly beneficial, by allowing the selection of appropriate control gains for the proposed controller leading to the desired behavior. Furthermore, based on the above analysis, this would enable the robot to continue walking and potentially reach steady-state, even under the presence of some error in the estimation of the ground stiffness magnitude.

Lastly, it has to be noted that the energy-based methodology proposed in this work depends on the model parameters of the system, as well as the selected optimal state-control pair of variables (x_0^*, u_0^*) . As a result, for a different model and gait parameters, the exhaustive grid searches (Fig. 6) would need to be repeated. Consequently, the identified optimal control gains for various ground stiffness values (Fig. 8), as well as the fitted nonlinear curves reported in this work (Table 2) would need to be recalculated. Nonetheless, it's crucial to emphasize that this computationintensive procedure is intended to be carried out offline, eliminating the need for any real-time computations during the actual locomotion of the target robot. Moreover, the suggested approach lends itself to offline implementation for a range of optimal statecontrol pairs (representing different gait parameters), hence facilitating the creation of a comprehensive gait library consisting of stabilizing controllers tailored to a particular robot [61,62]. In addition, the principles of the analysis presented in this work are generalizable and can be applied to various biped robots with different structures and parameters. As a result, the proposed methodology could be followed in order to first identify a set of optimal initial conditions that result in periodic left-right symmetric gait (7)-(8), then design an LQR feedback law to regulate state errors (9), after that identify the necessary optimal control gains of the proposed controller for different ground stiffness perturbations (3.1), and finally produce stable reference walking gaits for the bipedal robot in question. Specifically, stable reference trajectories for the CoM and the feet of the model would be generated, which in turn could be utilized for the real-time control of the physical robot through a task-space controller [21,23,24,63-65]. It should be noted that similar to previous works employing actuated versions of the 3D Dual-SLIP [21,23,66], the physical robot would not have to implement the actuation mechanism employed by the model to track the generated trajectories. Therefore, for this work, the robot is not required to adjust the stiffness of its legs, in order to track the reference CoM trajectories and footstep locations produced by the extended 3D Dual-SLIP model and the bio-inspired controller.

Based on our model analysis, locomotion over compliant terrains appears to be inherently linked to energy losses caused by ground damping. Specifically, as the ground becomes more compliant, it results in greater energy dissipation, necessitating higher leg stiffness for the 3D Dual-SLIP model to handle single steps on such surfaces. While bipedal robots using the proposed framework do not need to modify leg stiffness to manage low ground-stiffness

one-step perturbations, they will still encounter energy losses when traversing compliant terrains. In order to handle this consequence, compliant elements could be incorporated into the design of legged robots, as they improve efficiency, performance, and robustness against impacts and uncertainties [31,32,67]. However, the presence of compliance in robots can complicate their mechanical design and control [68]. For that reason, certain methodologies should be followed for the design of both the compliant components and the controllers to preserve the compliant nature of the system [17,67,69]. Therefore, by introducing compliant elements and implementing suitable control methodologies, the robustness of legged robots on compliant surfaces can be enhanced.

In conclusion, this paper proposes an energy-based framework for dynamic walking of bipeds across compliant surfaces, including extremely soft ones. An extended variation of the 3D Dual-SLIP model supporting locomotion over compliant terrain is utilized, while a novel bio-inspired controller is employed to regulate onestep unilateral perturbations of extremely low stiffness. Additionally, an energy-based methodology is introduced for the tuning of the bio-inspired controller to allow for dynamic walking with robustness across a wide range of low ground-stiffness one-step unilateral perturbations. Lastly, the extended model equipped with the proposed controller is shown to produce qualitatively humanlike vertical GRF responses even for locomotion over compliant terrain, while it succeeds handling even repeated unilateral stiffness perturbations under specific conditions. As stable walking with robustness across various very soft surfaces is an open problem in legged locomotion, this work can significantly advance the field of biped locomotion by generating stable walking trajectories for bipeds and humanoids traversing compliant terrains, whilst improving the robustness of lower-limb prostheses with adjustable stiffness.

Funding Data

- National Science Foundation (Grant Nos. #2020009, #2015786, #2025797, and #2018905; Funder ID: 10.13039/ 100000083).
- This scientific paper is partially supported by the Onassis Foundation (Scholarship ID: F ZQ029-1/2020-2021).

Data Availability Statement

The datasets generated and supporting the findings of this article are obtainable from the corresponding author upon reasonable request.

References

- Venancio, M. M., Gonalves, R. S., and Bianchi, R. A. D C., 2021, "Terrain Identification for Humanoid Robots Applying Convolutional Neural Networks," IEEE/ASME Trans. Mechatron., 26(3), pp. 1433–1444.
- [2] Wang, M., Wonsick, M., Long, X., and Padr, T., 2020, "In-Situ Terrain Classification and Estimation for NASA's Humanoid Robot Valkyrie," IEEE/ ASME International Conference on Advanced Intelligent Mechatronics (AIM), Boston, MA, July 6–9, pp. 765–770.
- [3] Li, C., Zhang, T., and Goldman, D. I., 2013, "A Terradynamics of Legged Locomotion on Granular Media," Science, 339(6126), pp. 1408–1412.
- [4] Torres-Pardo, A., Pinto-Fernández, D., Garabini, M., Angelini, F., Rodriguez-Cianca, D., Massardi, S., Tornero, J., Moreno, J. C., and Torricelli, D., 2022, "Legged Locomotion Over Irregular Terrains: State of the Art of Human and Robot Performance," Bioinspir. Biomim., 17(6), p. 061002.
- [5] Mesesan, G., Englsberger, J., Garofalo, G., Ott, C., and Albu-Schäffer, A., 2019, "Dynamic Walking on Compliant and Uneven Terrain Using Dcm and Passivity-Based Whole-Body Control," IEEE-RAS 19th International Conference on Humanoid Robots (Humanoids), Toronto, ON, Canada, Oct. 15–17, pp. 25–32.
- [6] Hopkins, M. A., Leonessa, A., Lattimer, B. Y., and Hong, D. W., 2016, "Optimization-Based Whole-Body Control of a Series Elastic Humanoid Robot," Int. J. Humanoid Rob. 13(11), p. 1550034
- Int. J. Humanoid Rob., 13(01), p. 1550034.
 [7] Hubicki, C., Abate, A., Clary, P., Rezazadeh, S., Jones, M., Peekema, A., Van Why, J., Domres, R., Wu, A., Martin, W., Geyer, H., and Hurst, J., 2018, "Walking and Running With Passive Compliance: Lessons From Engineering: A Live Demonstration of the ATRIAS Biped," IEEE Rob. Autom. Mag., 25(3), pp. 23–39.
- [8] Sabourin, C., Bruneau, O., and Buche, G., 2006, "Control Strategy for the Robust Dynamic Walk of a Biped Robot," Int. J. Rob. Res., 25(9), pp. 843–860.

- [9] Xiong, X., Ames, A. D., and Goldman, D. I., 2017, "A Stability Region Criterion for Flat-Footed Bipedal Walking on Deformable Granular Terrain," IEEE/RSJ International Conference on Intelligent Robots and Systems (IROS), Vancouver, BC, Canada, Sept. 24–28, pp. 4552–4559.
- [10] Wu, Y., Yao, D., and Xiao, X., 2018, "The Effects of Ground Compliance on Flexible Planar Passive Biped Dynamic Walking," J. Mech. Sci. Technol., 32(4), pp. 1793–1804.
- [11] Wu, Y., Yao, D., Guo, Z., and Xiao, X., 2019, "Adaptive Stiffness Control of Passivity-Based Biped Robot on Compliant Ground Using Double Deep Q Network," Proc. Inst. Mech. Eng., Part C: J. Mech. Eng. Sci., 233(6), pp. 2177–2189.
- [12] Yao, D., Yang, L., Xiao, X., and Zhou, M., 2022, "Velocity-Based Gait Planning for Underactuated Bipedal Robot on Uneven and Compliant Terrain," IEEE Trans. Ind. Electron., 69(11), pp. 11414–11424.
- [13] Bhattacharya, S., Luo, A., Dutta, S., Miura-Mattausch, M., and Mattausch, H. J., 2020, "Force-Sensor-Based Surface Recognition With Surface-Property-Dependent Walking-Speed Adjustment of Humanoid Robot," IEEE Access, 8, pp. 169640–169651.
- [14] Full, R. J., and Koditschek, D. E., 1999, "Templates and Anchors: Neuro-mechanical Hypotheses of Legged Locomotion on Land," J. Exp. Biol., 202(23), pp. 3325–3332.
- [15] Vasilopoulos, V., Paraskevas, I. S., and Papadopoulos, E. G., 2014, "Compliant Terrain Legged Locomotion Using a Viscoplastic Approach," IEEE/RSJ International Conference on Intelligent Robots and Systems, Chicago, IL, Sept. 14–18, pp. 4849–4854.
- [16] Gatthon, A., and Degani, A., 2020, "Minimalistic Control for Reaching Absolute State of a One-Legged Dynamic Robot on Uncertain Terrain," ASME J. Dyn. Syst. Meas. Control, 142(7), p. 071005.
- [17] Poulakakis, I., and Grizzle, J. W., 2009, "The Spring Loaded Inverted Pendulum as the Hybrid Zero Dynamics of an Asymmetric Hopper," IEEE Trans. Autom. Control, 54(8), pp. 1779–1793.
- [18] Thatte, N., and Geyer, H., 2016, "Toward Balance Recovery With Leg Prostheses Using Neuromuscular Model Control," IEEE Trans. Biomed. Eng., 63(5), pp. 904–913
- [19] Gong, Y., and Grizzle, J. W., 2022, "Zero Dynamics, Pendulum Models, and Angular Momentum in Feedback Control of Bipedal Locomotion," ASME J. Dyn. Syst. Meas. Control, 144(12), p. 121006.
- [20] Geyer, H., Seyfarth, A., and Blickhan, R., 2006, "Compliant Leg Behaviour Explains Basic Dynamics of Walking and Running," Proc. Royal Soc. B Biol. Sci., 273(1603), pp. 2861–2867.
- [21] Liu, Y., Wensing, P. M., Orin, D. E., and Zheng, Y. F., 2015, "Dynamic Walking in a Humanoid Robot Based on a 3D Actuated Dual-SLIP Model," IEEE International Conference on Robotics and Automation (ICRA), Seattle, WA, May 26–30, pp. 5710–5717.
- [22] Shahbazi, M., Saranl I, U., Babuška, R., and Lopes, G. A., 2016, "Approximate Analytical Solutions to the Double-Stance Dynamics of the Lossy Spring-Loaded Inverted Pendulum," Bioinspir. Biomim., 12(1), p. 016003.
- [23] Liu, Y., Wensing, P. M., Orin, D. E., and Zheng, Y. F., 2015, "Trajectory Generation for Dynamic Walking in a Humanoid Over Uneven Terrain Using a 3D-Actuated Dual-Slip Model," IEEE/RSJ International Conference on Intelligent Robots and Systems (IROS), Hamburg, Germany, Sept. 28–Oct. 2, pp. 374–380
- [24] Xiong, X., and Ames, A., 2021, "Slip Walking Over Rough Terrain Via h-Lip Stepping and Backstepping-Barrier Function Inspired Quadratic Program," IEEE Rob. Autom. Lett., 6(2), pp. 2122–2129.
- [25] Rummel, J., Blum, Y., Maus, H. M., Rode, C., and Seyfarth, A., 2010, "Stable and Robust Walking With Compliant Legs," IEEE International Conference on Robotics and Automation, Anchorage, AK, May 3–7, pp. 5250–5255.
- [26] Ernst, M., Geyer, H., and Blickhan, R., 2012, "Extension and Customization of Self-Stability Control in Compliant Legged Systems," Bioinspir. Biomim., 7(4), p. 046002.
- [27] Kerimoglu, D., Karkoub, M., Ismail, U., Morgul, O., and Saranli, U., 2021, "Efficient Bipedal Locomotion on Rough Terrain Via Compliant Ankle Actuation With Energy Regulation," Bioinspir. Biomim., 16(5), p. 056011.
- [28] Visser, L., Stramigioli, S., and Carloni, R., 2012, "Robust Bipedal Walking With Variable Leg Stiffness," Fourth IEEE RAS & EMBS International Conference on Biomedical Robotics and Biomechatronics (BioRob), Rome, Italy, June 24–27, pp. 1626–1631.
- [29] Visser, L. C., Stramigioli, S., and Carloni, R., 2013, "Control Strategy for Energy-Efficient Bipedal Walking With Variable Leg Stiffness," IEEE International Conference on Robotics and Automation, Karlsruhe, Germany, May 6–10, pp. 5644–5649.
- [30] Roozing, W., Visser, L. C., and Carloni, R., 2014, "Variable Bipedal Walking Gait With Variable Leg Stiffness," Fifth IEEE RAS/EMBS International Conference on Biomedical Robotics and Biomechatronics, Sao Paulo, Brazil, Aug. 12–15, pp. 931–938.
- [31] Liu, X., and Poulakakis, I., 2015, "On the Energetics of a Switchable Parallel Elastic Actuator Design for Monopedal Running," IEEE International Conference on Robotics and Biomimetics, Zhuhai, China, Dec. 6–9, pp. 769–774.
- [32] Liu, X., Rossi, A., and Poulakakis, I., 2018, "A Switchable Parallel Elastic Actuator and Its Application to Leg Design for Running Robots," IEEE/ASME Trans. Mechatron., 23(6), pp. 2681–2692.
- 33] Xie, S., Li, X., Zhong, H., Hu, C., and Gao, L., 2021, "Compliant Bipedal Walking Based on Variable Spring-Loaded Inverted Pendulum Model With Finite-Sized Foot," Sixth IEEE International Conference on Advanced Robotics and Mechatronics (ICARM), Chongqing, China, July 3–5, pp. 667–672.

- [34] Gaathon, A., and Degani, A., 2022, "Optimizing and Designing a Leg Shape to Increase Robustness of a Running Robot on Rough Terrain," Bioinspir. Biomim., 17(6), p. 066022.
- [35] Farley, C. T., Houdijk, H. H., Van Strien, C., and Louie, M., 1998, "Mechanism of Leg Stiffness Adjustment for Hopping on Surfaces of Different Stiffnesses," J. Appl. Physiol., 85(3), pp. 1044–1055.
- [36] Ferris, D. P., Louie, M., and Farley, C. T., 1998, "Running in the Real World: Adjusting Leg Stiffness for Different Surfaces," Proc. Royal Soc. London Ser. B: Biol. Sci., 265(1400), pp. 989–994.
- [37] Ferris, D. P., Liang, K., and Farley, C. T., 1999, "Runners Adjust Leg Stiffness for Their First Step on a New Running Surface," J. Biomech., 32(8), pp. 787–794.
 [38] Müller, R., Birn-Jeffery, A. V., and Blum, Y., 2016, "Human and Avian Running
- [38] Müller, R., Birn-Jeffery, A. V., and Blum, Y., 2016, "Human and Avian Running on Uneven Ground: A Model-Based Comparison," J. R. Soc. Interface, 13(122), p. 20160529.
- [39] Karakasis, C., Poulakakis, I., and Artemiadis, P., 2022, "Robust Dynamic Walking for a 3D Dual-SLIP Model Under One-Step Unilateral Stiffness Perturbations: Towards Bipedal Locomotion Over Compliant Terrain," 30th Mediterranean Conference on Control and Automation (MED), Vouliagmeni, Greece, June 28-July 1 pp. 969-975
- 28–July 1, pp. 969–975.
 [40] Bosworth, W., Whitney, J., Kim, S., and Hogan, N., 2016, "Robot Locomotion on Hard and Soft Ground: Measuring Stability and Ground Properties in-Situ," IEEE International Conference on Robotics and Automation (ICRA), Stockholm, Sweden, May 16–21, pp. 3582–3589.
- [41] Holgate, M. A., Sugar, T. G., and Bohler, A. W., 2009, "A Novel Control Algorithm for Wearable Robotics Using Phase Plane Invariants," IEEE International Conference on Robotics and Automation, Kobe, Japan, May 12–17, pp. 3845–3850.
- [42] Shepherd, M. K., and Rouse, E. J., 2017, "The VSPA Foot: A Quasi-Passive Ankle-Foot Prosthesis With Continuously Variable Stiffness," IEEE Trans. Neural Syst. Rehabil. Eng., 25(12), pp. 2375–2386.
- [43] Glanzer, E. M., and Adamczyk, P. G., 2018, "Design and Validation of a Semi-Active Variable Stiffness Foot Prosthesis," IEEE Trans. Neural Syst. Rehabil. Eng., 26(12), pp. 2351–2359.
- [44] Liu, Y., 2015, A Dual-SLIP Model for Dynamic Walking In a Humanoid Over Uneven Terrain, The Ohio State University, ProQuest Dissertations Publishing.
- [45] Skidmore, J., and Artemiadis, P., 2016, "Unilateral Walking Surface Stiffness Perturbations Evoke Brain Responses: Toward Bilaterally Informed Robot-Assisted Gait Rehabilitation," IEEE International Conference on Robotics and Automation (ICRA), Stockholm, Sweden, May 16–21, pp. 3698–3703.
- [46] Skidmore, J., Barkan, A., and Artemiadis, P., 2014, "Investigation of Contralateral Leg Response to Unilateral Stiffness Perturbations Using a Novel Device," IEEE/ RSJ International Conference on Intelligent Robots and Systems, Chicago, IL, Sept. 14–18, pp. 2081–2086.
- [47] Skidmore, J., Barkan, A., and Artemiadis, P., 2015, "Variable Stiffness Treadmill (VST): System Development, Characterization, and Preliminary Experiments," IEEE/ASME Trans. Mechatron., 20(4), pp. 1717–1724.
- IEEE/ASME Trans. Mechatron., 20(4), pp. 1717–1724.

 [48] Barkan, A., Skidmore, J., and Artemiadis, P., 2014, "Variable Stiffness Treadmill (VST): A Novel Tool for the Investigation of Gait," IEEE International Conference on Robotics and Automation (ICRA), Hong Kong, China, May 31–June 7, pp. 2838–2843.
- [49] Skidmore, J., and Artemiadis, P., 2016, "Unilateral Floor Stiffness Perturbations Systematically Evoke Contralateral Leg Muscle Responses: A New Approach to Robot-Assisted Gait Therapy," IEEE Trans. Neural Syst. Rehabil. Eng., 24(4), pp. 467–474
- [50] Frost, R., Skidmore, J., Santello, M., and Artemiadis, P., 2015, "Sensorimotor Control of Gait: A Novel Approach for the Study of the Interplay of Visual and Proprioceptive Feedback," Front. Human Neurosci., 9, p. 14.
 [51] Skidmore, J., and Artemiadis, P., 2016, "Sudden Changes in Walking Surface
- [51] Skidmore, J., and Artemiadis, P., 2016, "Sudden Changes in Walking Surface Compliance Evoke Contralateral EMG in a Hemiparetic Walker: A Case Study of Inter-Leg Coordination After Neurological Injury," 38th Annual International Conference of the IEEE Engineering in Medicine and Biology Society (EMBC), Orlando, FL, Aug. 16–20, pp. 4682–4685.

- [52] Skidmore, J., and Artemiadis, P., 2016, "On the Effect of Walking Surface Stiffness on Inter-Limb Coordination in Human Walking: Toward Bilaterally Informed Robotic Gait Rehabilitation," J. NeuroEng. Rehabil., 13(1), pp. 1–11.
 [53] Skidmore, J., and Artemiadis, P., 2015, "Leg Muscle Activation Evoked by Floor
- [53] Skidmore, J., and Artemiadis, P., 2015, "Leg Muscle Activation Evoked by Floor Stiffness Perturbations: A Novel Approach to Robot-Assisted Gait Rehabilitation," IEEE International Conference on Robotics and Automation (ICRA), Seattle, WA, May 26–30, pp. 6463–6468.
- [54] Skidmore, J., and Artemiadis, P., 2017, "Unilateral Changes in Walking Surface Compliance Evoke Dorsiflexion in Paretic Leg of Impaired Walkers," J. Rehabil. Assist. Technol. Eng., 4, p. 205566831773846.
 [55] Skidmore, J., and Artemiadis, P., 2019, "A Comprehensive Analysis of
- [55] Skidmore, J., and Artemiadis, P., 2019, "A Comprehensive Analysis of Sensorimotor Mechanisms of Inter-Leg Coordination in Gait Using the Variable Stiffness Treadmill: Physiological Insights for Improved Robot-Assisted Gait Therapy," IEEE 16th International Conference on Rehabilitation Robotics (ICORR), Toronto, ON, Canada, pp. 28–33.
- [56] Fukuchi, C. A., Fukuchi, R. K., and Duarte, M., 2018, "A Public Dataset of Overground and Treadmill Walking Kinematics and Kinetics in Healthy Individuals," PeerJ, 6, p. e4640.
- [57] Lee, H., Rouse, E. J., and Krebs, H. I., 2016, "Summary of Human Ankle Mechanical Impedance During Walking," IEEE J. Transl. Eng. Health Med., 4, pp. 1–7.
- [58] Au, S. K., and Herr, H. M., 2008, "Powered Ankle-Foot Prosthesis," IEEE Rob. Autom. Mag., 15(3), pp. 52–59.
- [59] Kim, M., and Collins, S. H., 2017, "Once-per-Step Control of Ankle Push-Off Work Improves Balance in a Three-Dimensional Simulation of Bipedal Walking," IEEE Trans. Rob., 33(2), pp. 406–418.
- [60] Chambers, V., and Artemiadis, P., 2021, "A Model-Based Analysis of Supraspinal Mechanisms of Inter-Leg Coordination in Human Gait: Toward Model-Informed Robot-Assisted Rehabilitation," IEEE Trans. Neural Syst. Rehabil. Eng., 29, pp. 740–749.
- [61] Da, X., Harib, O., Hartley, R., Griffin, B., and Grizzle, J. W., 2016, "From 2D Design of Underactuated Bipedal Gaits to 3D Implementation: Walking With Speed Tracking," IEEE Access, 4, pp. 3469–3478.
- [62] Hartley, R., Da, X., and Grizzle, J. W., 2017, "Stabilization of 3D Underactuated Biped Robots: Using Posture Adjustment and Gait Libraries to Reject Velocity Disturbances," IEEE Conference on Control Technology and Applications (CCTA), Maui, HI, Aug. 27–30, pp. 1262–1269.
- [63] Narkhede, K. S., Kulkarni, A. M., Thanki, D. A., and Poulakakis, I., 2022, "A Sequential MPC Approach to Reactive Planning for Bipedal Robots Using Safe Corridors in Highly Cluttered Environments," IEEE Rob. Autom. Lett., 7(4), pp. 11831–11838.
- [64] Xiong, X., and Ames, A. D., 2020, "Dynamic and Versatile Humanoid Walking Via Embedding 3d Actuated Slip Model With Hybrid Lip Based Stepping," IEEE Rob. Autom. Lett., 5(4), pp. 6286–6293.
- [65] Xiong, X., and Ames, A. D., 2019, "Motion Decoupling and Composition Via Reduced Order Model Optimization for Dynamic Humanoid Walking With Clf-qp Based Active Force Control," IEEE/RSJ International Conference on Intelligent Robots and Systems (IROS), Macau, China, Nov. 3–8, pp. 1018–1024.
- [66] Liu, Y., Wensing, P. M., Schmiedeler, J. P., and Orin, D. E., 2016, "Terrain-Blind Humanoid Walking Based on a 3-D Actuated Dual-SLIP Model," IEEE Rob. Autom. Lett., 1(2), pp. 1073–1080.
- [67] Sharbafi, M. A., Yazdanpanah, M. J., Ahmadabadi, M. N., and Seyfarth, A., 2020, "Parallel Compliance Design for Increasing Robustness and Efficiency in Legged Locomotion–Theoretical Background and Applications," IEEE/ASME Trans. Mechatron., 26(1), pp. 335–346.
- [68] Chen, J., Liang, Z., Zhu, Y., Liu, C., Zhang, L., Hao, L., and Zhao, J., 2019, "Towards the Exploitation of Physical Compliance in Segmented and Electrically Actuated Robotic Legs: A Review Focused on Elastic Mechanisms," Sensors, 19(24), p. 5351
- [69] Sreenath, K., Park, H.-W., Poulakakis, I., and Grizzle, J. W., 2011, "A Compliant Hybrid Zero Dynamics Controller for Stable, Efficient and Fast Bipedal Walking on MABEL," Int. J. Rob. Res., 30(9), pp. 1170–1193.